# Crystal structures of two phases of Pigment Yellow 110 from X-ray powder diffraction data

**Article** *in* Zeitschrift für Kristallographie – Crystalline Materials · March 2023

DOI: 10.1515/zkri-2023-0003



**3 authors**, including:

Jacco van de Streek
Avant-garde Materials Simulation
**157** PUBLICATIONS **17,129** CITATIONS
SEE PROFILE

Svetlana N. Ivashevskaya
Karelian Research Centre of the Russian Academy of Sciences
**37** PUBLICATIONS **473** CITATIONS
SEE PROFILE

Jacco van de Streek*, Svetlana N. Ivashevskaya and Martin U. Schmidt

# Crystal structures of two phases of Pigment Yellow 110 from X-ray powder diffraction data

https://doi.org/10.1515/zkri-2023-0003
Received January 29, 2023; accepted March 12, 2023;
published online March 23, 2023

**Abstract:** The crystal structure of the β-phase of Pigment Yellow 110 was determined from X-ray Powder Diffraction (XRPD) data. The crystal structure of the α-phase (Erk et al., *CrystEngComm* 2004, **6**, 474) is re-refined against the original XRPD data to modern-day standards. Dispersion-corrected density functional theory calculations are used to complement the powder data. The α- and β-form crystallise in $P\bar{1}$ and $P2_1/c$, respectively, with the P.Y. 110 molecule occupying a centre of symmetry in both forms. Both polymorphs are layered structures consisting of infinite chains of hydrogen-bonded molecules.

**Keywords:** DFT-D; Pigment Yellow 110; structure determination from powder diffraction data.

## 1 Introduction

Pigment Yellow 110 (P.Y. 110, $C_{22}H_6Cl_8N_4O_2$, (3′*Z*)-3,3′-(1,4-phenylenedinitrilo)-bis(4,5,6,7-tetrachloroisoindolin-1-one), see Scheme 1) is a member of the class of isoindolinone pigments, which have good light fastness, weather fastness, solvent resistance and migration resistance [1]. Several of these pigments are commercially available, and P.Y. 110 is produced by, for example, BASF. It affords very reddish shades of yellow. P.Y. 110 is resistant to bleeding and to heat (up to 290 °C). The paint industry uses it frequently as a colourant for industrial finishes and in automotive finishes, see Figure 1. The pigment is also applied in emulsion paints and in architectural paint [1].

Several polymorphs of P.Y. 110 are known. The form that is commercially prepared is the α-polymorph. The β-phase of P.Y. 110 is obtained by heating the α-phase in aromatic solvents such as nitrobenzene to more than 150 °C [2]. Similarly, heating the α-phase in trimellitic acid to 300 °C for 2 h results in the β-phase [3]. Apparently the β-phase is the thermodynamically stable phase at high temperatures. Nevertheless, the α-phase is used for the colouration of polymers, even at temperatures of 290 °C. It remains to be investigated if the pigment particles in the final polymer actually exhibit the α-phase or the β-phase.

Further crystal phases are described in patents. For example, treating α-P.Y. 110 in liquid ammonia at −33 °C yields the greenish-yellow γ-phase. This phase is also obtained with methylamine, dimethylamine or *n*-propylamine as solvent [4]. The δ-phase can be prepared in the following way: a dispersion of the α-phase in *o*-dichlorobenzene is treated with 20% methanolic KOH for 30 min at 50 °C. The resulting powder is dispersed in water, neutralised with 10% $H_2SO_4$, and subsequently heated in *o*-dichlorobenzene at 150 °C for 2 h [5]. When the α-phase of P.Y. 110 is treated with NaOMe in methanol at 65 °C, the ε-phase is obtained [6].

Pigments are not dissolved in their application media, but finely dispersed. As a consequence, their crystal structures are maintained in the product and the physical properties of the final product depend on the polymorphic form of the pigment; to understand these properties at the molecular level, knowledge of the crystal structures of the polymorphs is required. Like all organic pigments, P.Y. 110 is essentially insoluble in most solvents, and single crystals suitable for X-ray analysis are difficult or impossible to grow. Instead, crystal structures of organic pigments are frequently determined from X-ray Powder Diffraction (XRPD) data (see *e.g.* [7] for γ-Pigment Blue 15, ε-Pigment Blue 15, α-Pigment Yellow 110 and Pigment Yellow 139 [8], for Pigment Orange 2 and [9] for β-Pigment Orange 36, Pigment Orange 62, Pigment Yellow 151, α-Pigment Yellow 154, β-Pigment Yellow 181 and Pigment Yellow 194).

The crystal structure of the α-phase of P.Y. 110 was determined from laboratory XRPD data in 2004 [7]. The structural model of the α-polymorph was generated “in a less common way” through a combination of molecular modelling, intuition and Rietveld refinement [7]. Two final models were published: one resulting from calculations with a force field and one resulting from a free-atom Rietveld refinement without any constraints or restraints on the molecular geometry. As is to be expected for XRPD data, the

***Corresponding author: Jacco van de Streek**, Institute of Inorganic and Analytical Chemistry, Goethe University, Max-von-Laue-Str. 7, D-60438 Frankfurt am Main, Germany, E-mail: jaccovandestreek@yahoo.co.uk
**Svetlana N. Ivashevskaya,** Institute of Geology, Karelian Research Centre, Russian Academy of Sciences, Pushkinskaya 11, 185910 Petrozavodsk, Russia
**Martin U. Schmidt,** Institute of Inorganic and Analytical Chemistry, Goethe University, Max-von-Laue-Str. 7, D-60438 Frankfurt am Main, Germany

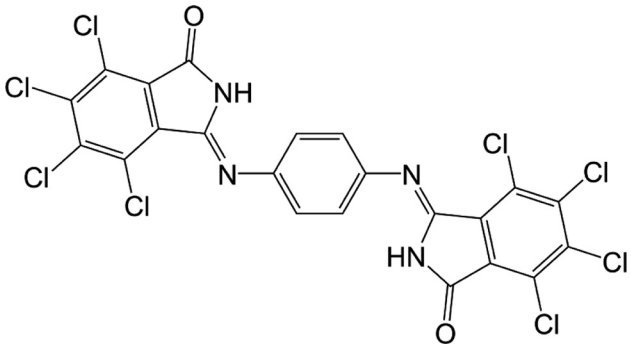


**Scheme 1:** The structural formula of P.Y. 110.


**Figure 1:** Car coated with P.Y. 110. The identity of the pigments in the coating was determined by mass spectrometry using the laser desorption ionisation technique. The coating additionally contains the benzimidazolone pigment P.Y. 154, the crystal structure of which was also determined by X-ray powder diffraction [9].

free refinement leads to a heavily distorted molecular geometry. The model from the force-field calculations is excellent from a chemical point of view, but due to the inaccuracies inherent in the force field approach, the agreement of the simulated and experimental powder data is worse, resulting in high *R*-values.

Molecular-modelling techniques and computer power have improved tremendously over the past decade, and the force-field techniques used at the time have been replaced by much more accurate, and much more time-consuming, quantum-mechanical calculations, namely by Dispersion-corrected Density Functional Theory (DFT-D) calculations [10].

In this publication we re-refined the known crystal structure of the α-phase, using a state-of-the-art combination of Rietveld refinement and DFT-D and we determined the crystal structure of the β-phase of P.Y. 110 from laboratory XRPD data.

# 2 Methods

## 2.1 Experimental

For the α-form, the original laboratory XRPD data from [7] were used. The measured sample had been prepared as follows: 20 g Cromophtal Yellow 2 RLP from BASF and 450 g nitrobenzene were stirred at 160 °C for 5 days. The powder was isolated by filtration, washed with methanol and dried on air at ambient conditions. The yield was 18.7 g (94%). The powder pattern was measured between 4° and 60° 2$\theta$ with steps of 0.02° in 2$\theta$. According to the original paper, the experimental data were "taken on a routine instrument" with Cu$K\alpha$ radiation. Based on our Rietveld refinement, variable slits were used, indicating a flat-plate geometry (Bragg–Brentano or reflection setup).

The β-phase of P.Y. 110 was prepared by heating 3 g of the α-phase of P.Y. 110 in 60 ml of *N*-methylpyrrolidone at 203 °C in suspension for 2 h. The pigment was isolated by filtration, washed with ethanol and water, and dried at 80 °C *in vacuo*. The yield was 2.4 g (80%). The powder was measured on an STOE STADI-P diffractometer with Cu$K\alpha_1$-radiation (curved Ge(111) primary monochromator; $\lambda$ = 1.5406 Å) in a capillary in transmission geometry using a linear position-sensitive detector in the range between 2° and 70° with steps of 0.01° in 2$\theta$. For data acquisition the STOE software $WINX^{POW}$ [11] was used.

## 2.2 Structure solution and refinement

The crystal structures were solved in real space with *DASH* [12]. For structure solution, the powder patterns were truncated to a real-space resolution of around 2.5 Å, which for Cu$K\alpha_1$ radiation corresponds to 35° 2$\theta$. The background was subtracted with a high-pass filter [13]. The expected molecular volume in the solid state was calculated as 612 Å$^3$ using the atomic volumes from [14]. The first 20 peaks in the patterns were manually selected and fitted with *DASH* to obtain high precision peak positions. The powder patterns were indexed with the program *DICVOL91* [15]. The P.Y. 110 molecule has a centre of symmetry and could therefore occupy an inversion centre in the crystal structure. For the α-form, the space group was determined to be $P\bar{1}$, $Z'$ = ½ based on volume considerations. The space group of the β-form was determined to be $P2_1/c$, $Z'$ = ½ based on Bayesian analysis of the extinctions [16] and volume considerations. With the unit-cell parameters and the space group known, integrated intensities and their correlations were extracted in a Pawley fit [17].

A *Z*-matrix corresponding to half a P.Y. 110 molecule was created. The *Z*-matrix has one flexible torsion angle, which combined with three orientational degrees of freedom corresponds to a total of four degrees of freedom. The structure was solved by simulated annealing using *DASH*. To assess the reproducibility of the simulated annealing, 100 simulated annealing runs were run for each of the two forms.

Rietveld refinement was carried out with *TOPAS* [18] using all diffraction data, *i.e.* 1.54 Å real-space resolution for the α-phase and 1.34 Å real-space resolution for the β-phase. To ensure that the Rietveld refinement is as robust and smooth as possible, it was carried out in stages, gradually releasing more and more parameters. The first two stages consisted of Pawley refinements to establish suitable starting values for the unit-cell parameters and the peak-shape functions, which were then transferred to the Rietveld refinement. In the last cycle, all parameters were refined simultaneously, a requirement for the proper evaluation of the goodness of fit, which

depends on the number of parameters that is included in the fit. Anisotropic peak broadening and peak asymmetry were included to allow the peak profiles to be described accurately. One global $U_{iso}$ value was refined for all C, N and O atoms and one global $U_{iso}$ value was refined for the Cl atoms. The $U_{iso}$ for the H atoms was fixed at 1.2 times the $U_{iso}$ for the C, N and O atoms. Suitable chemical restraints were applied for all bond lengths, valence angles and the planarity of the central phenyl ring and the isoindolinone system. Since in both polymorphs the molecule is situated on a special position (an inversion centre), the asymmetric unit in principle contains only three of the six carbon atoms of the central phenyl ring. However, the three symmetry-related carbon atoms missing from the list of atoms prevent the addition of a planarity restraint for the phenyl ring as a whole, as well as the addition of one of the bond-length restraints and of four of the valence-angle restraints. This is sometimes solved by putting a dummy atom at the special position, keeping the position of the dummy atom fixed and adding bonds from the dummy atom to the three remaining carbon atoms of the phenyl ring. We used a different approach: the three missing carbon atoms were added to the asymmetric unit and the occupancies of all six carbon atoms were set to ½. However, the *x*, *y* and *z* coordinates of the three symmetry-related carbon atoms were linked by constraints to those of the three carbon atoms in the true asymmetric unit, *i.e.* the three additional carbon atoms are not allowed to move independently. In *TOPAS*, this is possible by defining nine variables and expressing the coordinates of all six carbon atoms in terms of these nine variables. Obviously, the number of degrees of freedom does not change, and all restraints can now be expressed in natural variables such as the carbon–carbon bond length without the need for converting a carbon–carbon bond length to the equivalent carbon-dummy bond length and setting a proper weight for these bond lengths. Inclusion of a March–Dollase preferred orientation correction [19] significantly improved the Rietveld fit for both phases.

## 2.3 Energy-minimisation

The crystal structures were energy-minimised with Dispersion-corrected Density Functional Theory (DFT-D) with the program *GRACE* [20], which calls *VASP* [21–23] for single-point pure DFT calculations with the Perdew–Burke–Ernzerhof (PBE) functional [24] and adds the Grimme 2010 dispersion correction [10] and a robust minimisation algorithm. The energy cut-off was set to 520 eV, the *k*-point spacing was approximately 0.07 $Å^{-1}$. The unit-cell parameters are included in the energy-minimisation, but the experimental space-group symmetry is imposed. This combination of DFT functional and dispersion correction, abbreviated as PBE-D3, has been thoroughly validated to accurately reproduce experimental single-crystal structures of organic compounds [25]. Incorrect structures distort when energy-minimised, and the degree of distortion upon energy-minimisation with the unit cell free, expressed as the root-mean-square Cartesian displacement (RMSCD) of the non-hydrogen atoms, can be used as an approximate quantitative measure for the reliability of the crystal structure. “Cartesian displacement” is not uniquely defined when the unit cells of the two crystal structures to be compared are different, as is the case for our calculations in which the unit cell is allowed to vary as part of the DFT-D optimisation. We define the Cartesian displacement Δ for an atom in two crystal structures as

$$\Delta = (|\mathbf{G}_1 \cdot \mathbf{r}_1 - \mathbf{G}_1 \cdot \mathbf{r}_2| + |\mathbf{G}_2 \cdot \mathbf{r}_1 - \mathbf{G}_2 \cdot \mathbf{r}_2|)/2 \quad (1)$$

where $\mathbf{r}_i$ are the fractional coordinates of the atoms in crystal structure *i*, and $\mathbf{G}_i$ is the transformation matrix from fractional to Cartesian coordinates for crystal structure *i*. This definition of Cartesian displacement has the advantages that it is symmetric with respect to the two structures to be compared, that it varies smoothly upon smooth distortions of either or both of the two structures to be compared, and that there is no need for a user-defined parameter such as the number of molecules used for the comparison. From the validation study on 225 experimental single-crystal structures, it was established that an RMSCD value smaller than 0.25 Å indicates that a crystal structure is correct.

Further details about the energy minimisation, the RMSCD and the validation study can be found in [25] and references therein.

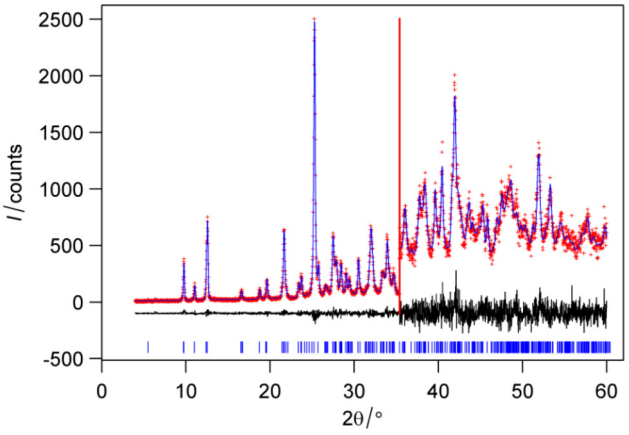


**Figure 2:** α-P.Y. 110. Fit of the calculated to the experimental PXRD pattern after Rietveld refinement (*x*-axis: °2*θ*; *y*-axis: counts). Calculated (blue), observed (red), and difference (black) profiles are shown. Tick marks are shown at the bottom of the profile. At 35.38° the scale changes by a factor of 6.

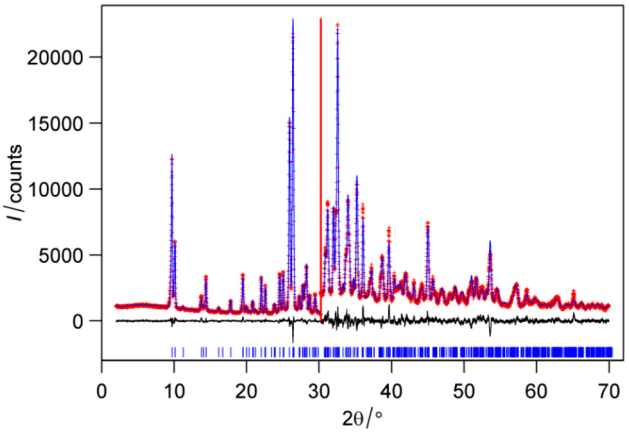


**Figure 3:** β-P.Y. 110. Fit of the calculated to the experimental PXRD pattern after Rietveld refinement (*x*-axis: °2*θ*; *y*-axis: counts). Calculated (blue), observed (red), and difference (black) profiles are shown. Tick marks are shown at the bottom of the profile. At 30.24° the scale changes by a factor of 4.

**Table 1:** Structural parameters of the Rietveld refinements of two P.Y. 110 structures (α-polymorph and β-polymorph) determined from powder diffraction data.

| | α-P.Y. 110 | β-P.Y. 110 |
|---|---|---|
| **Crystal data** | | |
| Chemical formula | $C_{22}H_6Cl_8N_4O_2$ | $C_{22}H_6Cl_8N_4O_2$ |
| $M_r$ | 641.94 | 641.94 |
| Crystal system, space group | Triclinic, $P\bar{1}$ | Monoclinic, $P2_1/c$ |
| Temperature (K) | 300 | 298 |
| $a$, $b$, $c$ (Å) | 9.588(3), 16.699(6), 3.8633(13) | 9.2153(3), 18.1774(4), 7.25753(15) |
| $\alpha$, $\beta$, $\gamma$ (°) | 91.010(6), 99.169(7), 105.490(5) | 90.00, 108.9328(17), 90.00 |
| $V$ (Å$^3$) | 587.3(4) | 1149.94(5) |
| $\rho$ (g/cm$^3$) | 1.815 | 1.854 |
| $Z$, $Z'$ | 1, ½ | 2, ½ |
| Radiation type | Cu$K\alpha$ | Cu$K\alpha_1$ |
| Wavelength of incident radiation (Å) | 1.54186 | 1.5406 |
| Specimen shape, size (mm) | – | Cylinder, 8 × 0.5 |
| **Data collection** | | |
| Diffractometer | – | STOE-Stadi-P |
| Specimen mounting | Flat plate | Glass capillary |
| Scan method | Continuous | Continuous |
| Data-collection mode | Reflection | Transmission |
| $2\theta$ values (°) | $2\theta$ min = 4.00, $2\theta$ max = 60.00, $2\theta$ step = 0.02 | $2\theta$ min = 2.00, $2\theta$ max = 69.99, $2\theta$ step = 0.01 |
| **Refinement** | | |
| $R_p$, $R_{wp}$, $R_{exp}$, $\chi^2$ | 11.717, 14.974, 13.546, 1.222 | 8.499, 9.644, 5.939, 2.637 |
| Excluded region(s) | None | None |
| No. of data points | 2801 | 6800 |
| No. of parameters | 130 | 102 |
| H-atom treatment | Restrained | Restrained |
| No. of restraints | 62 | 62 |

The high-angle part of a powder pattern, which contains the atomic-resolution data, suffers from peak overlap and low intensities. The reduced information content of this part of the pattern can be supplemented with information from the energy-minimised structures by adding geometrical parameters from the relevant energy-minimised polymorph as restraints to the Rietveld refinement. After the initial Rietveld refinement and the energy-minimisation, a final Rietveld refinement was therefore carried out with such "polymorph-dependent restraints" [26].

# 3 Results & discussion

Indexing of the α-form was troublesome, as described by [7], and several attempts were necessary. The fact that the unit cell is triclinic plays a role, but the problems are probably at least in part also due to the sample-displacement error, which cannot be corrected for prior to indexing and which manifests itself in the form of an unexpectedly large apparent zero-point error of 0.08° $2\theta$, unavoidably causing problems for the indexing algorithms. Indexing of the β-form was straightforward.

Simulated annealing resulted in 45 out of 100 correct solutions for α and 100 out of 100 correct solutions for β. The Rietveld plots are shown in Figures 2 and 3, the results are summarised in Table 1.

The RMSCD values between the experimental and the energy-minimised structures were 0.15 Å and 0.066 Å for α and β respectively, indicating that both crystal structures are correct.

The crystal structure of the α-phase of P.Y. 110 as published [7], is confirmed with dispersion-corrected density functional theory to be correct and precise. The RMSCD between their published structure and our re-refinement is only 0.11 Å, even though their structural model was generated almost two decades ago by Haddow "in a less common way" using molecular modelling.

The crystal structures of the α-phase and β-phase are very similar. In both polymorphs the molecules are situated on a centre of symmetry. Both forms contain virtually the same infinite chain of hydrogen-bonded molecules with the 2-pyrrolidone groups forming hydrogen bonds across an inversion centre along the **a**-axis (Figure 4). The angles between the phenyl ring and the isoindolinone moiety are

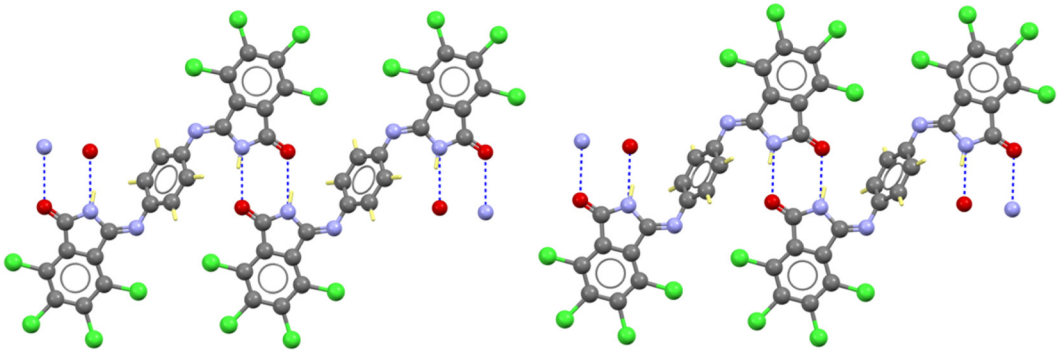

**Figure 4:** Hydrogen bonding in the α (left) and β (right) form of P.Y. 110.

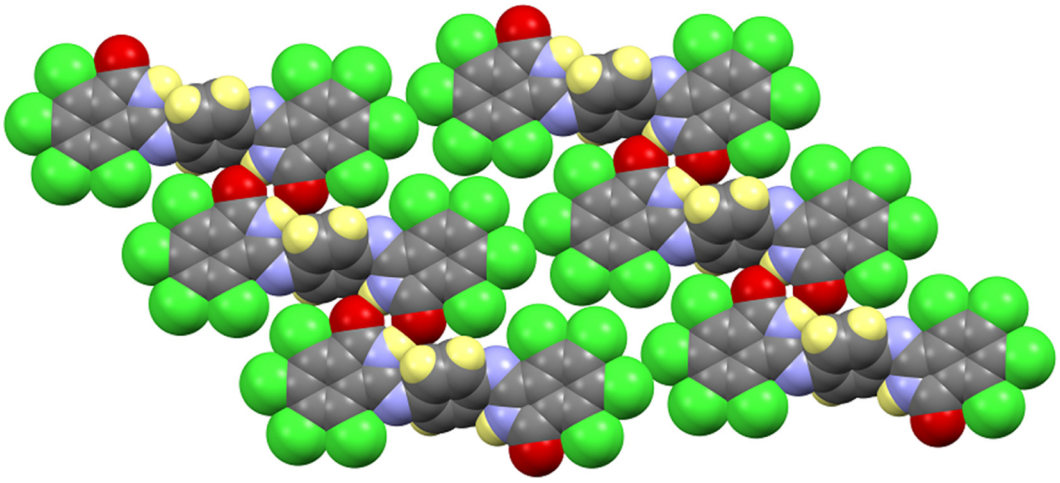

**Figure 5:** Packing of the infinite chains of hydrogen-bonded molecules into 2D layers in the α-form.

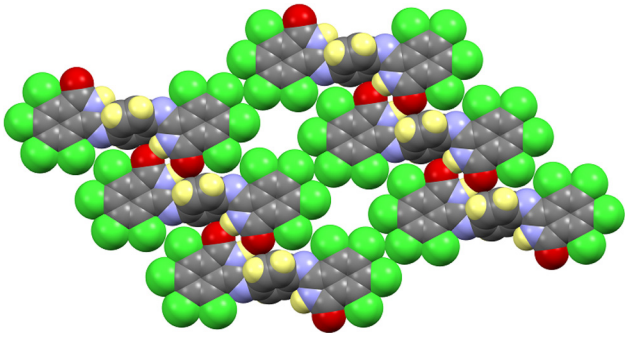

**Figure 6:** Packing of the infinite chains of hydrogen-bonded molecules into 2D layers in the β-form.

slightly different in the α- and β-forms: 50.8° and 61.7° respectively. This difference in the twist of the molecule is related to the different 2D packings (Figures 5 and 6). The 2D layers in both forms assemble into a layered structure (Figures 7 and 8). The main difference between the two polymorphs is therefore the arrangement of the hydrogen-bonded chains with respect to each other. In the β-phase, the 2D layers alternate their orientation in the **c** direction because of the presence of the $2_1$-screw axis. The difference in the two γ angles causes adjacent chains in the **b** direction to be offset by *ca*. 5 Å, as can be seen in Figures 5 and 6.

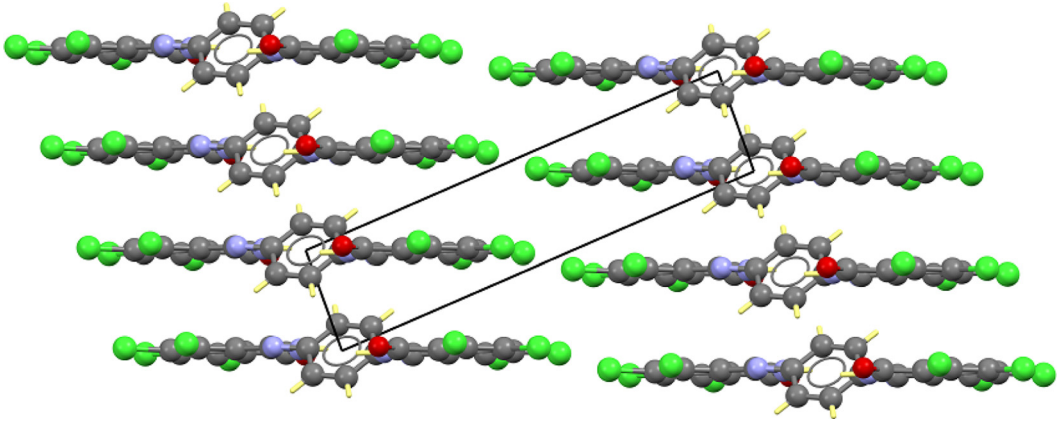

**Figure 7:** Layer structure of α-P.Y. 110. View along **a**, *i.e.* along the infinite chains of hydrogen-bonded molecules.

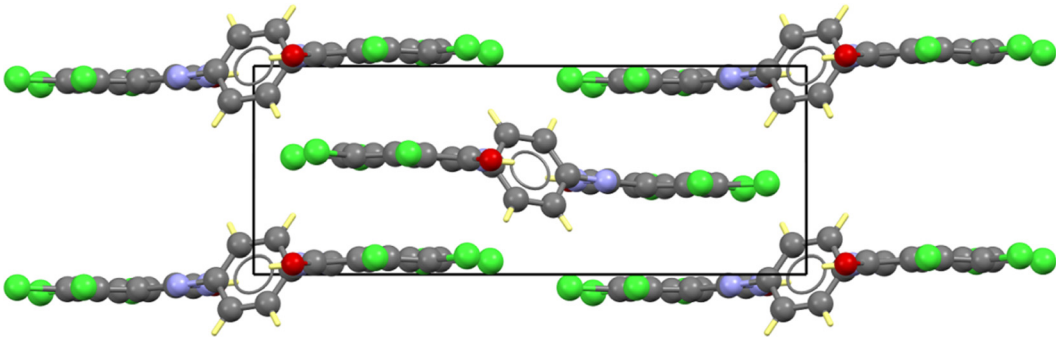

**Figure 8:** Layer structure of β-P.Y. 110. View along **a**, *i.e.* view along the infinite chains of hydrogen-bonded molecules.

## 4 Conclusions

The crystal structure of the α-phase of P.Y. 110 as published [7], even though the structural model was generated nearly two decades ago "in a less common way" using molecular modelling with an empirical force field, is confirmed by state-of-the art Rietveld refinement, and with dispersion-corrected density functional theory to be correct and precise.

The crystal structure of the β-phase was successfully solved from laboratory powder diffraction data using real-space methods with the program *DASH* followed by Rietveld refinement with *TOPAS*.

The crystal structures of the α-phase and β-phase are very similar. In both polymorphs the molecules are situated on a centre of symmetry. Both forms contain virtually the same infinite chain of hydrogen-bonded molecules across centres of symmetry, which in both forms assemble into layers. The only difference is the relative arrangements of the infinite chains of hydrogen-bonded molecules.

## Supplementary Material

Full details of the crystal structure determinations in cif format are available in the online version, at doi: https://doi.org/10.1515/zkri-2015-1910, and have also been deposited with the Cambridge Crystallographic Data Centre with deposition numbers 1483895 and 1483896. Copies of these can be obtained free of charge on written application to CCDC, 12 Union Road, Cambridge, CB2 1EZ, UK (fax: +44 1223 336033); on request by e-mail to deposit@ccdc.cam.ac.uk or by access to http://www.ccdc.cam.ac.uk.

**Acknowledgements:** Peter Erk (BASF) is gratefully acknowledged for providing the original X-ray powder data of the α-phase of P.Y. 110. Tanja Reipen and Hans-Walter Stein (Clariant, now Heubach, Frankfurt) are gratefully acknowledged for the preparation of the β-phase of P.Y. 110. Edith Alig (Goethe University, Frankfurt) is gratefully acknowledged for the collection of the powder diffraction pattern of the β form. JvdS gratefully acknowledges the Villum Foundation (Denmark) for financial support (project no. VKR023111) for hardware and software. SNI gratefully acknowledges a grant from the *Deutscher Akademischer Austauschdienst* (DAAD) through the "*Forschungsaufenthalte für Hochschullehrer und Wissenschaftler*" programme in 2007. Avant-garde Materials Simulation GmbH (Germany) is gratefully acknowledged for providing a complimentary copy of *GRACE*. Crystal structures were visualised using *Mercury* [27].

**Author contributions:** All the authors have accepted responsibility for the entire content of this submitted manuscript and approved submission.

**Research funding:** None declared.

**Conflict of interest statement:** The authors declare no conflicts of interest regarding this article.

## References

1. Hunger K., Schmidt M. U. *Industrial Organic Pigments: Production, Properties, Applications*; Wiley-VCH: Weinheim, 2018.
2. Ohoka S., Ohki Yamaguchi S. I. Yellow Pigment for Polyolefins. Japanese Patent JP 58001150 B4, 1975.
3. Momoi Y., Yamane M., Yamaguchi I. Yellow Pigment for Polyolefins. Japanese Patent JP 58001151 B4, 1975.
4. Baebler F. Neue stabile Modifikation eines Isoindolinon-Pigments. Verfahren zu deren Herstellung und deren Verwendung. German Patent DE 2804062, 1978.
5. Dainippon Ink. Yellow Isoindolinone Pigment. Japanese Patent JP 55065257 A2, 1978.
6. Dainippon Ink. Yellow Isoindolinone Pigment. Japanese Patent JP 63049711, 1981.
7. Erk P., Hengelsberg H., Haddow M. F., Van Gelder R. The innovative momentum of crystal engineering. *CrystEngComm* 2004, *6*, 474–483.

8. Yatsenko A. V., Paseshnichenko K. A., Chernyshev V. V., Schenk H. 1-[(2-Nitro-phenyl)-hydrazono]-1*H*-naphthalen-2-one (Pigment Orange 2) from powder data. *Acta Crystallogr.* 2001, *E57*, o1152–o1153.
9. Van de Streek J., Brüning J., Ivashevskaya S. N., Ermrich M., Paulus E. F., Bolte M., Schmidt M. U. Structures of six industrial benzimidazolone pigments from laboratory powder diffraction data. *Acta Crystallogr.* 2009, *B65*, 200–211.
10. Grimme S., Antony J., Ehrlich S., Krieg H. J. A consistent and accurate *ab initio* parametrization of density functional dispersion correction (DFT-D) for the 94 elements H-Pu. *Chem. Phys.* 2010, *132*, 154104-1–154104-19.
11. STOE & Cie. *WINXPOW*; STOE & Cie GmbH: Darmstadt, 2004.
12. David W. I. F., Shankland K., Van de Streek J., Pidcock E., Motherwell W. D. S., Cole J. C. *DASH*: a program for crystal structure determination from powder diffraction data. *J. Appl. Crystallogr.* 2006, *39*, 910–915.
13. Brückner S. Estimation of the background in powder diffraction patterns through a robust smoothing procedure. *J. Appl. Crystallogr.* 2000, *33*, 977–979.
14. Hofmann D. W. M. Fast estimation of crystal densities. *Acta Crystallogr.* 2002, *B57*, 489–493.
15. Boultif A., Louër D. Indexing of powder diffraction patterns for low-symmetry lattices by the successive dichotomy method. *J. Appl. Crystallogr.* 1991, *24*, 987–993.
16. Markvardsen A. J., David W. I. F., Johnson J. C., Shankland K. A probabilistic approach to space-group determination from powder diffraction data. *Acta Crystallogr.* 2001, *A57*, 47–54.
17. Pawley G. S. Unit-cell refinement from powder diffraction scans. *J. Appl. Crystallogr.* 1981, *14*, 357–361.
18. Coelho A. A. *TOPAS* and *TOPAS-Academic*: an optimization program integrating computer algebra and crystallographic objects written in C++. *J. Appl. Crystallogr.* 2018, *51*, 210–218.
19. Dollase W. A. Correction of intensities for preferred orientation in powder diffractometry: application of the March model. *J. Appl. Crystallogr.* 1986, *19*, 267–272.
20. Neumann M. A. *Grace Version 2.1*; Avant-garde Materials Simulation SARL: France, 2013.
21. Kresse G., Hafner J. *Ab initio* molecular dynamics for liquid metals. *Phys. Rev.* 1993, *B47*, 558–561.
22. Kresse G., Furthmüller J. Efficient iterative schemes for *ab initio* total-energy calculations using a plane-wave basis set. *Phys. Rev.* 1996, *B54*, 11169–11186.
23. Kresse G., Joubert D. From ultrasoft pseudopotentials to the projector augmented-wave method. *Phys. Rev.* 1999, *B59*, 1758–1775.
24. Perdew J. P., Burke K., Ernzerhof M. Generalized gradient approximation made simple. *Phys. Rev. Lett.* 1996, *77*, 3865–3868.
25. Van de Streek J., Neumann M. A. Validation of molecular crystal structures from powder diffraction data with DFT-D. *Acta Crystallogr.* 2014, *B70*, 1020–1032.
26. Van de Streek J. The crystal structure of Pigment Yellow 181 dimethylsulfoxide *N*-methyl-2-Pyrrolidone solvate (1:1:1) from XRPD + DFT-D. *Acta Crystallogr.* 2015, *B71*, 89–94.
27. Macrae C. F., Sovago I., Cottrell S. J., Galek P. T. A., McCabe P., Pidcock E., Platings M., Shields G. P., Stevens J. S., Towler M., Wood P. A. Mercury 4.0: from visualization to analysis, design and prediction. *J. Appl. Crystallogr.* 2020, *53*, 226–235.